coatings

MDPI

Article

Oxidation of Silicon Carbide Composites for Nuclear Applications at Very High Temperatures in Steam

Martin Steinbrueck [1,*], Mirco Grosse [1], Ulrike Stegmaier [1], James Braun [2] and Christophe Lorrette [2]

[1] Institute for Applied Materials (IAM-AWP), Karlsruhe Institute of Technology (KIT), 76344 Eggenstein-Leopoldshafen, Germany; mirco.grosse@kit.edu (M.G.); ulrike.stegmaier@kit.edu (U.S.)
[2] Université Paris-Saclay, CEA, Service de Recherches Métallurgiques Appliquées, 91 191 Gif-sur-Yvette, France; James.braun@cea.fr (J.B.); christophe.lorrette@cea.fr (C.L.)
* Correspondence: martin.steinbrueck@kit.edu; Tel.: +49-721-608-22517

Abstract: Single-rod oxidation and quench experiments at very high temperatures in steam atmosphere were conducted with advanced, nuclear grade SiC_f/SiC CMC cladding tube segments. A transient experiment was performed until severe local degradation of the sample at maximum temperature of approximately 1845 °C. The degradation was caused by complete consumption of the external CVD-SiC sealcoat, resulting in steam access to the fiber–matrix composite with less corrosion resistance. Approaching these very high temperatures was accompanied by accelerated gas release mainly of H_2 and CO_2, the formation of surface bubbles and white smoke. Three one-hour isothermal tests at 1700 °C in steam with final water flooding and one three-hour experiment with fast cool-down in Ar atmosphere were run under nominally identical conditions. All isothermally tested samples survived the tests without any macroscopic degradation. The mechanical performance of these quenched clad segments was not significantly affected, while maintaining a high capability to tolerate damages. Despite these harsh exposure conditions, load transfer between SiC fibers and matrix remained efficient, allowing the composites to accommodate deformation.

Keywords: silicon carbide; ceramic matrix composite; nuclear fuel cladding; high-temperature oxidation; water steam; mechanical properties

Citation: Steinbrueck, M.; Grosse, M.; Stegmaier, U.; Braun, J.; Lorrette, C. Oxidation of Silicon Carbide Composites for Nuclear Applications at Very High Temperatures in Steam. *Coatings* **2022**, *12*, 875. https://doi.org/10.3390/coatings12070875

Academic Editor: Csaba Balázsi

Received: 12 May 2022
Accepted: 15 June 2022
Published: 21 June 2022

1. Introduction

Silicon carbide (SiC) ceramic matrix composites (CMC) are candidates for accident-tolerant fuel (ATF) cladding used in light water reactors (LWR), promising the highest survival temperature in severe accident scenarios. They offer excellent mechanical properties at high temperatures, low density, as well as high oxidation and irradiation resistance. However, as ceramic materials, they are one of the most revolutionary approaches for new cladding tubes and other structural materials in nuclear reactors with a number of challenges that need to be addressed [1]. With this aim, CEA (Commissariat à l'Energie Atomique et aux Energies Alternatives) has systematically improved the original process to produce viable and robust nuclear grade SiC_f/SiC composites.

Intended applications of these new materials are for cladding tubes in gas-cooled fast reactors (GFR) and LWRs. The expected GFR operating conditions are helium as coolant at a pressure of 8 MPa and temperatures up to 1000 °C. Although the helium is expected to be of high purity, a low amount of impurities like oxygen, water, nitrogen, and others, is unavoidable in a technical system like a nuclear reactor. Higher temperatures may occur in hypothetical accident scenarios. A study on the behavior of SiC CMC cladding under these conditions was recently published [2]. Under LWR operating conditions (ca. 300 °C, 15 MPa), which are not discussed in this paper, hydrothermal corrosion of SiC is a major concern to be addressed [1,3]. In hypothetical accident scenarios after loss of coolant, high temperatures beyond 1000 °C in steam atmospheres can be rapidly reached. Under such conditions, conventional zirconium alloy claddings react strongly with steam, leading to

serious mechanical degradation of the fuel cladding and consequent loss of barrier effect against the release of fission products. In addition, the oxidation of Zr alloys by steam is associated with the release of hydrogen and heat, both of which greatly affect the course of a severe accident. Silicon carbide has the potential to perform significantly better under severe nuclear accident conditions, but experimental data with SiC-based prototypical cladding tubes at very high temperatures in steam atmospheres are still scarce to prove it.

This paper presents and discusses results of oxidation experiments up to 1850 °C with SiC_f/SiC CMC cladding segments manufactured by CEA, relevant to cope with severe accident scenarios in LWRs. The experiments were performed at KIT; post-test examinations were done in both institutes. The paper is based on a preliminary one presented at the TOPFUEL2021 conference [4] complemented by two more experiments and a more detailed discussion of the complete test series. The paper starts with a summary of the state of knowledge on high-temperature oxidation of silicon carbide in steam.

2. Overview on SiC Oxidation at High Temperatures

Silicon carbide ceramics are intensively studied because of their potential for application as high-temperature structural material. They offer excellent high-temperature mechanical properties, low density as well as high oxidation and irradiation resistance. The high-temperature oxidation resistance relies on the formation of a protective SiO_2 scale.

SiC is the only binary solid compound in the Si-C system. It is highly covalent with tetrahedral arrangement of C atoms around Si atoms (and vice versa) in closed packed atomic planes. More than 200 different crystal structures (polymorphs) of silicon carbide are reported. The two major polytypes are the metastable α-SiC having hexagonal crystal structure (similar to Wurtzite) and the thermodynamically stable β-SiC with a cubic zinc blende crystal structure (similar to diamond). The decomposition temperature is very high at around 2830 °C. A large number of papers have been published on silicon carbide and its behavior at high temperatures, e.g., by Snead [5] and by Presser [6]. Reviews with special attention to the high-temperature oxidation behavior of SiC in steam were published by Narushima [7], Opila [8], Roy [9], and Pham [10].

Silica formed during oxidation of SiC also exists in several polymorphs—the amorphous phase and various crystalline phases. The crystalline phases are, from the low-temperature to the high-temperature, quartz, tridymite, and cristobalite, respectively. The melting temperature of SiO_2 is around 1725 °C, softening of the amorphous phase starts already below 1600 °C. The Pilling–Bedworth ratio, i.e., the ratio between the SiO_2 and the SiC substrate volumes, is approximately one, leading to a good bond at the interface with a very small stress build-up at the SiC/SiO_2 interface [5]. On the other hand, the coefficients of thermal expansion of amorphous SiO_2 and of β-cristobalite are lower and higher, respectively, than that of SiC [11], which may lead to stresses in the silica scale during changes in temperature.

The oxidation of SiC in steam-containing atmospheres is complex compared, e.g., to the oxidation of zirconium alloys. Its high-temperature oxidation resistance relies on the formation of a protective silicon oxide layer according to Equations (1) and (2). The formation of methane, CH4, is theoretically also possible, but practically negligible at the high temperatures and water vapor partial pressures discussed here. Hydrogen is released in addition to carbon-containing gases. At higher temperatures, the formation of volatile hydroxides or oxyhydroxides may take place, e.g., according to Equations (3) and (4). Furthermore, silicon monoxide, SiO, may be formed at low oxygen partial pressures and high temperatures, Equation (5). Formation and volatilization of a silica layer at the same time finally leads to paralinear oxidation kinetics, as illustrated in Figure 1 and described by Equation (6).

$$SiC + 3H_2O(g) = SiO_2 + CO(g) + 3H_2(g) \quad (1)$$

$$SiC + 4H_2O(g) = SiO_2 + CO_2(g) + 4H_2(g) \quad (2)$$

$$SiO_2 + 2H_2O(g) = Si(OH)_4(g) \quad (3)$$

$$SiO_2 + H_2O(g) = SiO(OH)_2(g) \quad (4)$$

$$SiO_2 = SiO(g) + 0.5O_2(g) \quad (5)$$

$$\frac{dX}{dt} = \frac{k_p}{2X} - k_l \quad (6)$$

with X being oxide thickness, t time, k_p parabolic rate constant, and k_l linear rate constant.

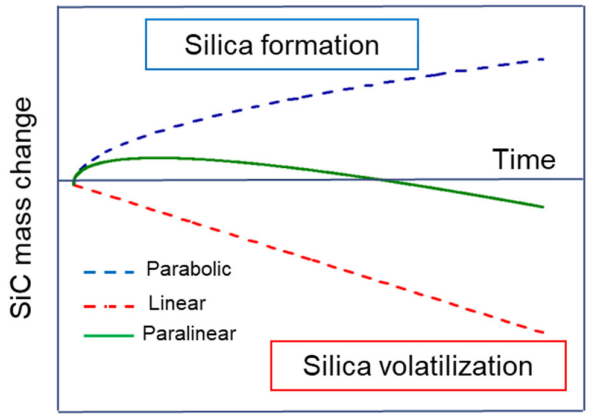

Figure 1. Paralinear mass change during HT oxidation of SiC due to formation and volatilization of a superficial SiO_2 scale.

The parabolic growth rate of silica in steam in the absence of volatilization is around one order of magnitude faster than in dry oxygen atmosphere due to about 10 times larger permeability of H_2O and OH^- molecules in SiO_2, according to Opila [12]. Terrani [13] published a correlation for the SiO_2 thickness during parabolic oxidation of SiC in steam. The linear volatilization rate is strongly dependent on total pressure, steam partial pressure, and gas flow velocity. Corresponding relations were also published in [13,14].

Only a few literature sources deal with high-temperature oxidation of SiC-based CMC cladding in steam. Without going into detail, Yueh and Terrani [15] tested CVD coated SiC_f/SiC specimens in steam between 1200 and 1700 °C. After 4 h of exposure at 1 atm pressure, no significant weight change was detected at 1200 and 1600 °C, and only a small weight loss was detected at 1700 °C. Terrani [13] published results of steam oxidation of various SiC samples between 1200 and 1700 °C and varying pressure between 0.1 and 2 MPa. Identical oxidation behavior was found between monolithic CVD SiC and CVD coated SiC fibers composites, as long as the environmental barrier coating (EBC) remained intact. On the other hand, non-coated SiC_f/SiC composites were strongly degraded. Steam oxidation of CVD SiC up to 1700 °C resulted in uniform materials recession with slow kinetics (<1 mg/cm^2/h). Steam oxidation as a function of its partial pressure of different SiC CMC samples up to 2000 °C including final quenching by water was investigated by Avincola [16]. For lower steam partial pressures (10–30 kPa), the parabolic constants (k_p) were in agreement with the data from literature obtained at lower temperatures. At 1600 °C and 60 kPa, the mass gain became irregular due to the formation of bubbles, which increased with exposure time and steam partial pressure. Despite bubble formation, all samples remained intact with only minor superficial degradation. Furthermore, one-hour oxidation tests at 1700 and 1800 °C resulted in silica layers of around 2 µm. Most of the samples oxidized in steam during ramp tests from 1400 to 2000 °C (10 K/min) withstood even quenching by water [16].

The formation of bubbles in the silica scale was also observed by other authors [12–14,17], showing increasing tendency for bubble formation along with increasing temperature and steam partial pressure.

Finally, it should be mentioned that impurities in the furnace, the sample, or the oxidizing atmosphere might strongly affect oxidation kinetics. This is one of the reasons why published data on high-temperature oxidation of silicon carbide are so scattered. The

oxidation process is accelerated by the presence of impurities and residual sintering additives, which affect the microstructure of the protective SiO_2 scale. Opila and Jacobson [8] discussed the strong effect of low-level impurities from alumina furnace tubes on the oxidation kinetics. Such Al impurities change the structure and transport properties of the silica scale and affect the apparent oxidation activation energy. In addition, alkali metal impurities (e.g., sodium and potassium) in the oxidation environment may have a strong effect because they are silica network modifiers. A detailed discussion of the influence of these and other impurities on the oxidation behavior is given in [8].

3. Materials and Methods

3.1. Samples

Five 6 cm long SiC_f/SiC samples were manufactured by CEA. The composite materials consist of CVI-SiC_f/SiC tubes processed in the standard LWR nuclear fuel assembly geometry. Third generation Hi-Nicalon type S fibers (NGS Advanced Fibers Co., LTD, Toyama-Shi, Japan) were employed as reinforcement. Two successive fibers layers at ±45° were applied by filament winding to confer the material mechanical performances. The SiC matrix was chemically vapor infiltrated by a CVI process after deposition of a thin pyrocarbon (PyC) interphase (50–100 nm) until a high-density level. Complete coverage of the fiber reinforcement was achieved. The inner and outer CVD SiC surfaces were then ground to meet dimension requirements. The final porosity volume fraction was below 10%. More details about the manufacturing process can be found in [18]. The samples were filled with graphite (used as a susceptor for the high-frequency (HF) inductive heating purpose [16]) and tightly sealed with end caps at both sides (Figure 2).

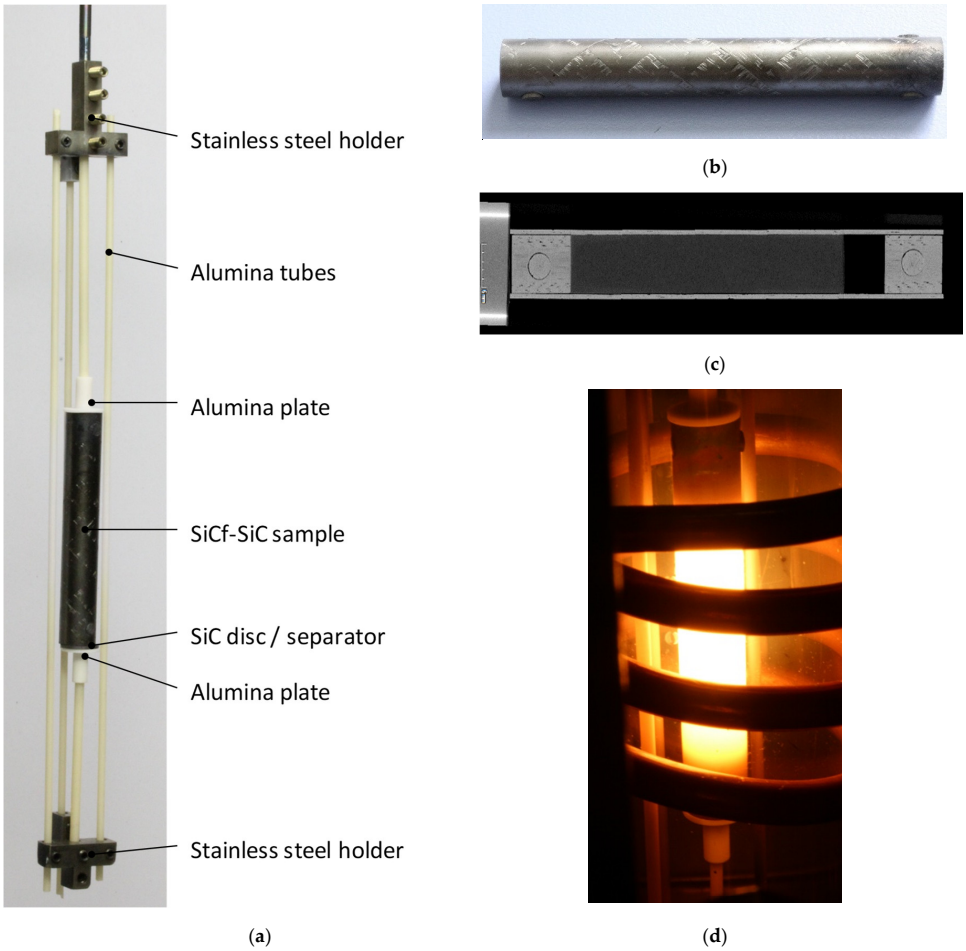

Figure 2. QUENCH-SR facility and SiC_f-SiC sample. (**a**) Sample holder; (**b**) SiC_f/SiC sample before test; (**c**) SiC_f-SiC sample before test (tomography); (**d**) Sample in QUENCH-SR rig at 1700 °C.

3.2. Test Facility and Conduct

The oxidation experiments were conducted in the QUENCH-SR (single rod) facility at KIT with inductive heating and the possibility of quenching the samples by water. In this facility, the samples are enclosed in a quartz glass tube allowing observation of the test by video recording. A water-cooled copper coil surrounding the glass tube generates a magnetic field inducing eddy currents in the graphite susceptor, Figure 2. Power (max. 20 kW) is provided by an HF generator working at a frequency up to 700 kHz. Temperature is measured and controlled via a two-color pyrometer (type IGAR 12-LO MB22) working at the wavelengths 1.28 and 1.65 µm with a measuring range of 500 to 2200 °C.

Gas supply was controlled by a Bronkhorst® system consisting of gas flow controller, water flow controller, and a CEM (controlled evaporator and mixer). Furthermore, 40 L/h argon flowed through the facility throughout all tests, and 60 g/h steam was injected during the oxidation phases resulting in a steam concentration of 65 vol.% at normal pressure. The Ar and steam injection resulted in a gas flow velocity of approximately 5 cm/s in the quartz glass tube section.

The off-gas line is connected to a mass spectrometer (MS, IPI GAM 3000, InProcess Instruments Gesellschaft für Prozessanalytik mbH, Bremen, Germany) for quantitative measurement of H_2O, H_2, CO, CO_2, CH_4, and other gases with Ar as reference. The MS was calibrated for all relevant gases before the tests.

The transient test (SiC-01) was conducted from 600 °C until failure of the sample with steam switched on at 1400 °C. The heating rate was 10 K/min during the whole test. The test was ended by switching off power and the steam flow after first indication of strong degradation, i.e., local hot spot, high concentrations of reaction gases and fume production. Hence, the sample quickly cooled down in a humid argon flow without quenching.

Three identical isothermal tests (SiC-02, SiC-03, and SiC-05) were conducted for one hour at 1700 °C. These samples were used for various destructive post-test examinations. The samples were heated from 600 to 1700 °C with a rate of 1 K/s in argon. Steam flow was switched on approximately 90 s after reaching the isothermal plateau. The tests were terminated by quenching with a rising cylinder filled with water at 95 °C at a quench rate of approximately 1 cm/s. The power supply was switched off when the water level reached the lower end of the sample. Test SiC-04 was run for three hours and fast cool-down in (humid) argon gas flow (no water quenching), but otherwise under identical conditions.

All tests were video recorded during the oxidation phases in steam. A snapshot of such a video is shown in Figure 2d. A summary of test parameters, post-test examinations, and some relevant results is provided in Table 1.

Table 1. Test characteristics, post-test examinations conducted, and selected results.

	SiC-01	SiC-02	SiC-03	SiC-04	SiC-05
Type	transient	isothermal	isothermal	isothermal	isothermal
Time, h	0.75	1	1	3	1
Test end	gas cooling	water quench	water quench	gas cooling	water quench
PTE	yes	no	yes	yes	no
Mech. Tests	no	yes	no	no	yes
H_2 release, mL	250	267	231	469 161 *	287
SiO_2, µm	0–3		0.5–1.6	2.7–3.9	

* Hydrogen release after 1 h oxidation.

3.3. Post-Test Examinations

The pre- and post-test appearance was documented non-destructively by photography (Canon EOS 1200D, Canon Inc., Tokio, Japan), SEM/EDS (FEI XL30S with Silicon Drift Detector EDS detector, FEI Company, Eindhoven, The Netherlands), and X-ray tomography (Phoenix v | *tome* | xs *240*, GE Sensing & Inspection Technologies GmbH, Wunstorf, Germany).

The ramp-tested (SiC-01) and two isothermally tested (SiC-03 and SiC-04) samples were cut longitudinally, embedded in epoxy resin, ground and polished for ceramographic analyses of the cross sections, named PTE (post-test examination) in Table 1.

Uniaxial tensile tests were performed at room temperature on the isothermally oxidized samples SiC-02 and SiC-05 to assess the residual mechanical behavior and performances. Mechanical tests coupled with acoustic emission (EA) monitoring were carried out up to failure in accordance with the ISO 20323 standard, followed by an SEM analysis of the fracture surfaces. Cycled tensile tests were conducted on reference samples and SiC-05 to give information on the damage progression. Thus, the reduced modulus, the hysteresis loops with area, and the residual strains were extracted from the experimental curves. Details about the procedure can be found in [18]. The samples strain was locally measured by means of a class 1 extensometer with a gauge length of 25 mm. The SiC-05 sample was coated with a grey painting to also determine the strain by Direct Image Correlation (DIC) in accordance with ASTM E2208-02.

4. Results

4.1. Transient Test until Failure

The inductive heating via the graphite core and the pyrometer control of temperature worked well up to the highest temperature. The temperature history and the main results of the MS measurements for the SiC-01 test are summarized in Figure 3.

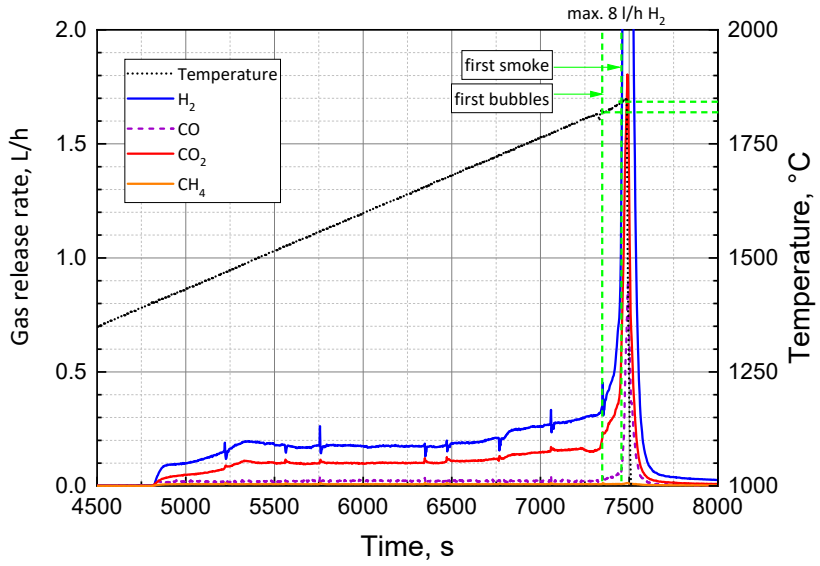

Figure 3. Temperature history and gas release rates during transient test SiC-01.

The oxidation rate was in-situ measured by the gas concentrations, which were converted into release rates using the Ar flow rate as reference. The releases of hydrogen and CO_2, and to a lesser extent of CO, were immediately observed when the steam injection started at 1400 °C. A very low signal of methane, CH_4, appeared throughout the test. H_2 and CO_2 release rates increased up to 1490 °C and then remained more or less constant up to 1730 °C. From 1730 to 1820 °C, a linear increase of gas release rates was observed before a strong oxidation escalation resulted in a fast increase of gas release rates up to termination of the test. Interestingly, the CO release rate only increased beyond 1820 °C.

First bubbles at the sample surface were observed at 1820 °C; first visual indication of smoke formation was at 1840 °C. The test was stopped by switching off power and steam injection after stronger development of smoke in the test section at the maximum temperature of 1845 °C. The smoke was most probably caused by severe volatilization of SiO and Si-O-H species from the hot sample surface and their immediate oxidation and condensation in colder parts of the test section. Figure 4 provides some snapshots taken from the video approaching the end of the experiment. They show the formation of bubbles

(3rd–5th image) and smoke (5th image). Closer views on bubble formation during the isothermal tests at 1700 °C are shown later in Figure 9.

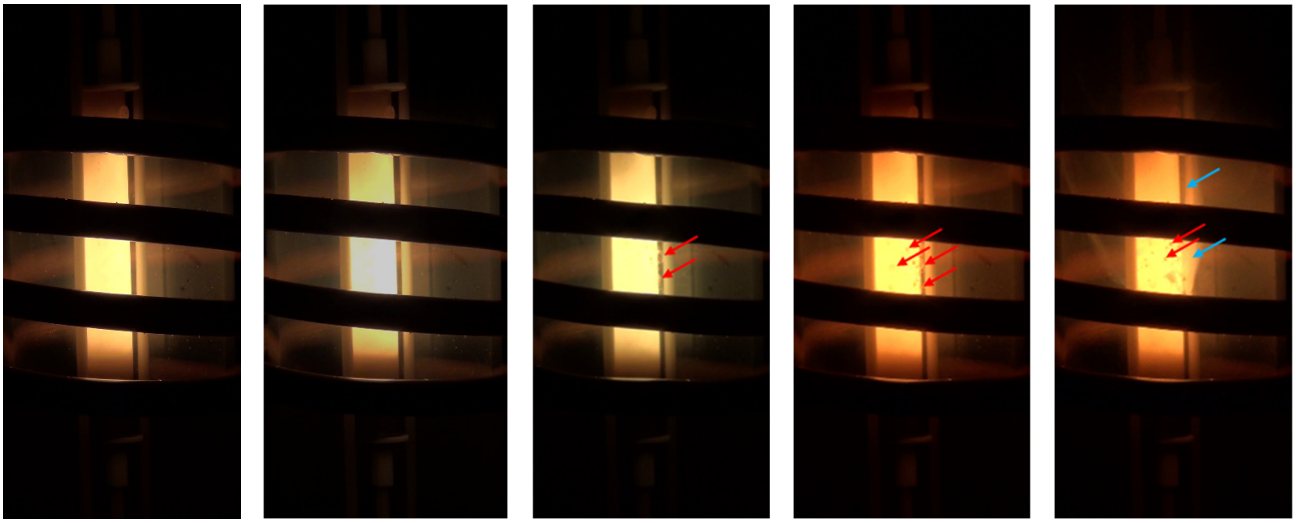

Figure 4. Video snapshots taken at the times and temperatures given during transient test SiC-01. Red arrows show positions of bubbles, blue ones the formation of smoke.

Visual and Ceramographic Post-Test Examinations

The sample is locally degraded in the area assumed to have the highest temperature level as it can be seen in Figure 5. However, it is not broken and has retained its geometric integrity. No sign of through-wall degradation and corresponding steam attack of graphite was seen by X-ray tomography and later on by ceramography.

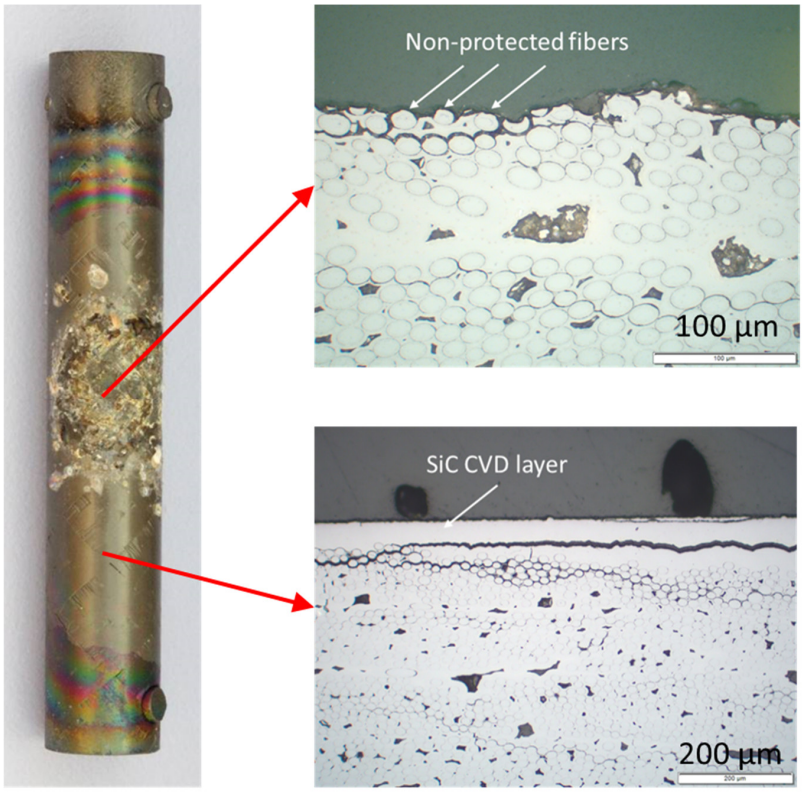

Figure 5. Post-test appearance of the sample after the transient test up to 1845 °C and optical micrographs from the failure region in the middle of the sample and from the non-failure region below.

Locally, the external CVD SiC layer was consumed/removed, most probably resulting in the high gas release rates as shown in Figure 3. The optical micrographs in Figure 5 clearly show that the fibers in the damage region are exposed, and that they have interacted with the steam atmosphere. About half of the tube wall thickness was consumed in this region as it is seen in the X-ray tomography image in Figure 6. The reaction of steam with the pyrocarbon interphase as well as the much higher effective surface of the fiber-matrix composite should be the main reasons for the accelerated oxidation kinetics resulting in high gas release rates. At lower and higher positions of the sample (with lower temperatures), the external CVD layer remained intact. In those areas, a 2–3 µm thick silica scale was measured by SEM/EDS.

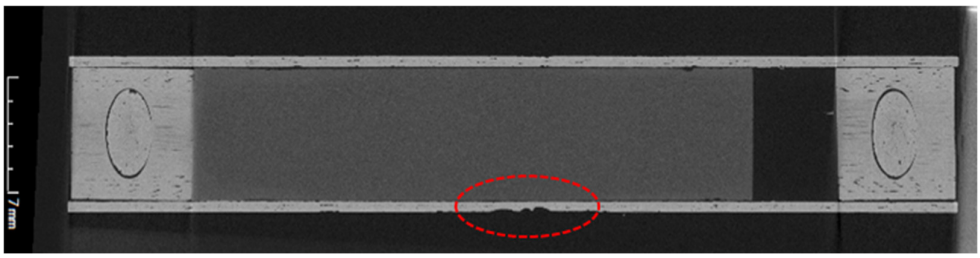

Figure 6. X-ray tomography (longitudinal cut) of the sample after the transient test up to 1845 °C.

4.2. Isothermal Tests at 1700 °C

All isothermal tests ran under nominally the same conditions with respect to temperature and gas/steam flow rates. The visual observation during the tests (also video recorded) showed slight irregularities at the surface of the samples, including dark dots, which could be caused by the formation of small bubbles. The formation of one big bubble was seen in test SiC-03 after approximately 16 min in the steam phase, which reached its maximum size 4 min later and remained stable for approximately 30 min. Bubbles of different size were also observed during the other isothermal tests and later on confirmed by post-test examinations, see Figure 9.

Gas release rates of relevant gases (H_2, CO_2, CO, and CH_4) are presented in Figure 7. H_2 and CO_2, according to Equation (2), are the main gaseous reaction products, followed by CO and a very low amount of methane, CH_4. This reaction gas composition is in correspondence to what is thermodynamically expected at 1700 °C for excess of steam conditions. However, it cannot be ruled out that the gas composition changed during transport from the place of production at 1700 °C to the mass spectrometer with an inlet temperature of approximately 150 °C. The release rates vary slightly for the different tests, which is also reflected by the figures for the integral release of the gases; see Table 1 for H_2. The integral data include gas release during the quenching phases, which contributed 10, 15, and 3 mL hydrogen for the tests SiC-02, SiC-03, and SiC-05, respectively. The different values result from slightly different times for switching off the heating power and flooding of the samples. The reason for the variations of gas release rates between the tests during the isothermal phase is not clear but may be related to slightly different sample temperatures, e.g., due to different gaps between the SiC tube and the graphite rod or different surface conditions for instance by the availability of bubbles at the measurement spot of the pyrometer.

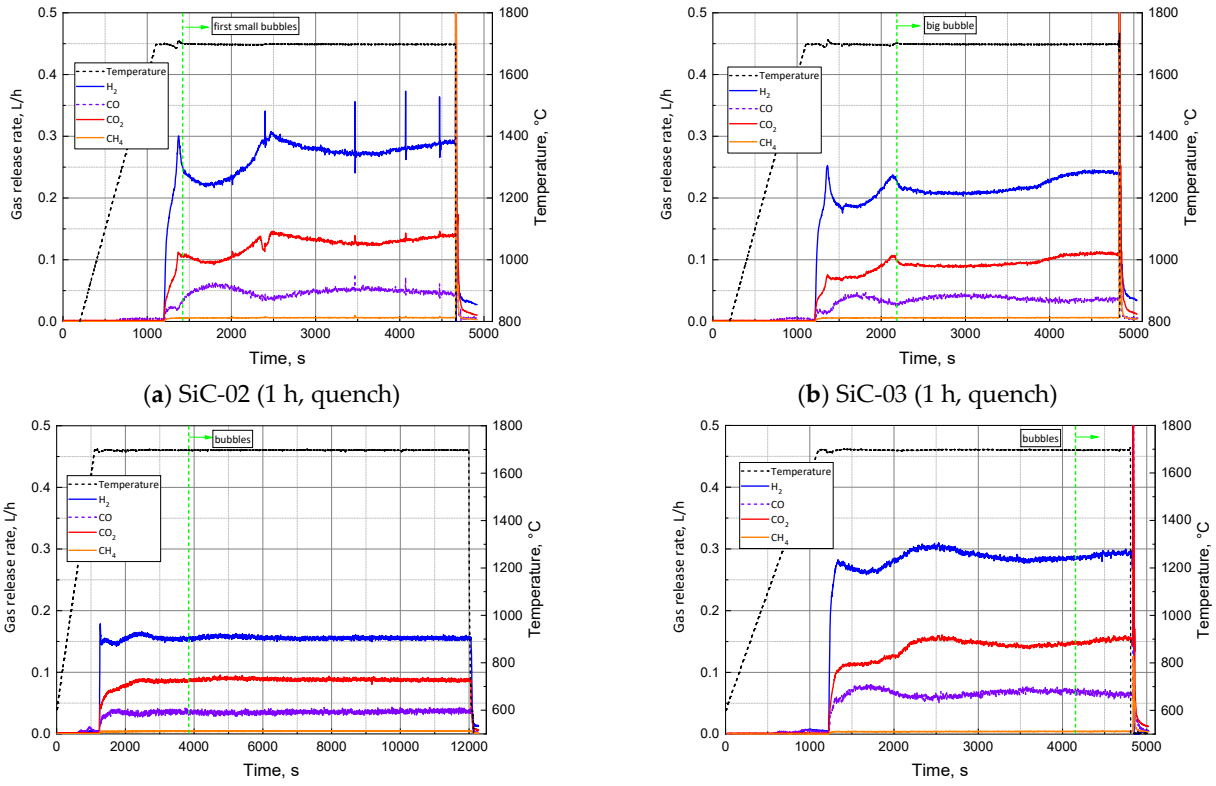

(**a**) SiC-02 (1 h, quench)

(**b**) SiC-03 (1 h, quench)

(**c**) SiC-04 (3 h, cool-down in Ar)

(**d**) SiC-05 (1 h, quench)

Figure 7. Temperature history and gas release rates during the isothermal tests at 1700 °C.

The detailed trend of the gas flow curves is very similar for all tests, with an initial (simultaneous to steam injection) sharp increase for all gases, followed by a slight reduction and increase again for hydrogen and carbon dioxide. This behavior should be connected with the initial formation and stabilization of the silica scale. The CO curve follows a somehow opposite behavior in these phases. The following slight variations of the gas release signals could be caused by the formation of bubbles. The 3-h lasting test SiC-04 shows a very stable gas release after approximately 45 min. All release rates of the produced gases sharply increase with initiation of the quench process as discussed above. The gas release at the end of test SiC-04 with fast cooling in (humid) argon flow rapidly decreases to very low values with switching off the heating power.

The mass change of all isothermally tested samples was relatively low, being slightly negative for samples SiC-02/-03 and slightly positive for SiC-04/-05. There is no obvious correlation between mass change and other test parameters and results. It could be connected to a different degree of spalling of SiO_2 bubbles during quenching.

4.2.1. Post-Test Examinations

The post-test appearance of all isothermally tested samples is very similar, see Figure 8. The integrity and geometry have been preserved, despite some slight alterations compared to the as-received samples. The surface appears stained and tempering colors are seen at the ends of the tube segments. The latter result from the temperature gradient toward the ends of the samples (without graphite susceptor) and indicate thin silica scales with changing thickness in the order of magnitude of the light wavelengths. Remnants of large bubbles are visible to the naked eye.

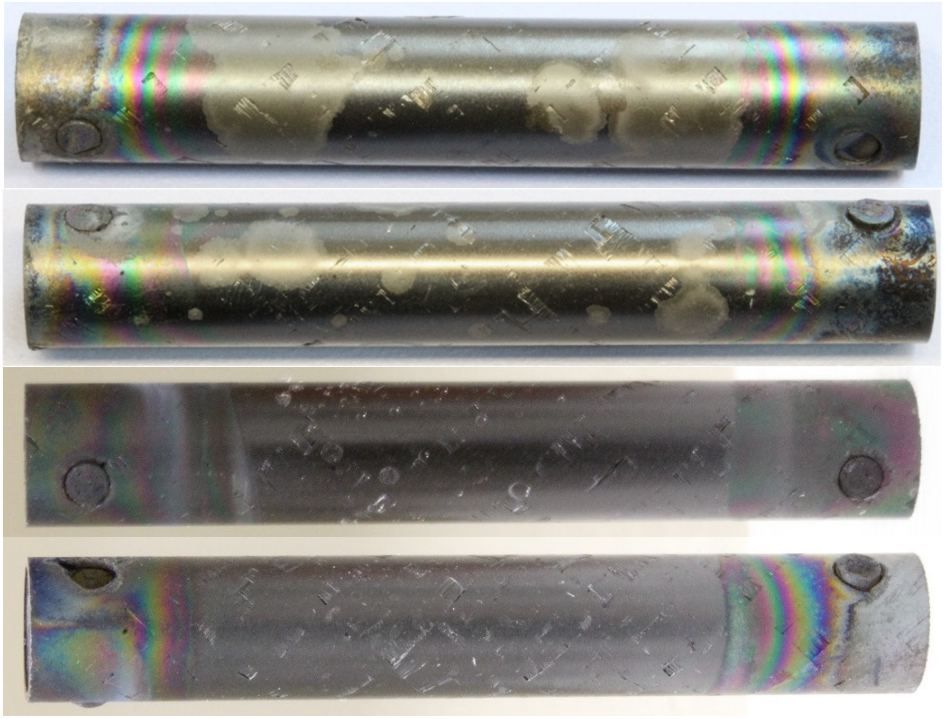

Figure 8. Post-test appearance of the samples after 1 h (3 h for SiC-04) isothermal oxidation at 1700 °C in steam.

X-ray tomography with its limited resolution showed no degradation of the SiC tube segments, neither externally from the interaction with steam nor internally due to interaction with the graphite susceptor.

Representative SEM images of typical sample surfaces with bubbles from various samples as well as one video snapshot taken during test SiC-04 are provided in Figure 9. The images show closed and burst bubbles as well as their remnants of various sizes ranging from a few micrometers to almost one millimeter. The bubbles on sample SiC-04 (Figure 9c) are 2–3 mm in size. It should be mentioned that these images have been taken at selected areas with bubbles; there were also larger areas covered by a smooth silica layer without bubbles. The images are just examples of various types of bubbles and not necessarily typical for only the specific sample where they are from. EDS analyses of the samples' surfaces showed only peaks of Si and O with the composition of SiO_2.

The images in Figure 10 show cross section micrographs of samples SiC-03 and SiC-04 obtained by optical microscopy and SEM. As expected from the online and tomography results, the CVD-SiC sealcoat remained intact during 1-h as well as 3-h oxidation at 1700 °C. Furthermore, no indications of interaction between SiC and graphite (susceptor) were found. The SiO_2 scale produced by the oxidation of SiC was around 1 µm thick with single measurement values between 0.5 and 1.6 µm for the SiC-03 sample and 2.7–3.9 µm for the SiC-04 sample. Taking into account the roughly constant gas release rates during the isothermal tests, it could be assumed that the oxide scale thicknesses correspond to the equilibrium value of the paralinear oxidation determined by growth and volatilization of SiO_2 [19]. The oxide thicknesses measured on these samples correspond well to other data published for oxidation of SiC in steam at 1700 °C [13,14,16], which are all in the range of a few micrometers at this temperature.

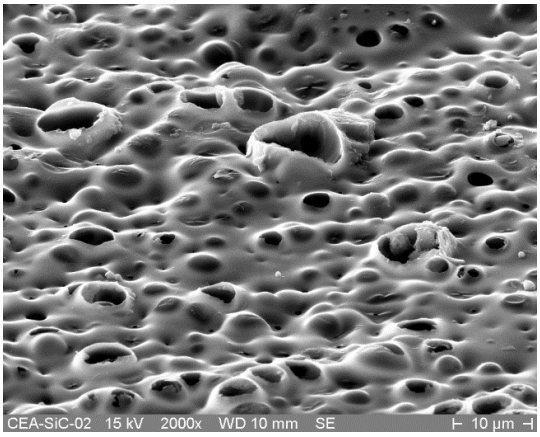

(**a**) SiC-02

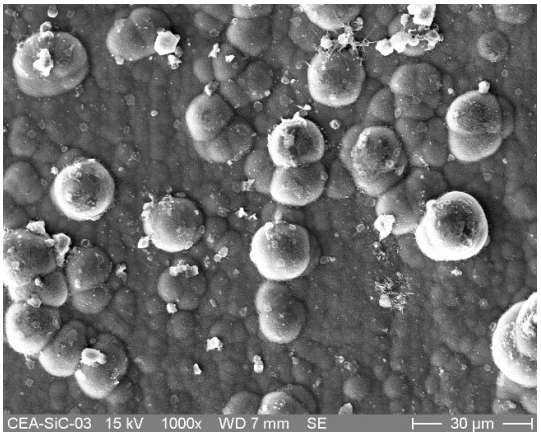

(**b**) SiC-03

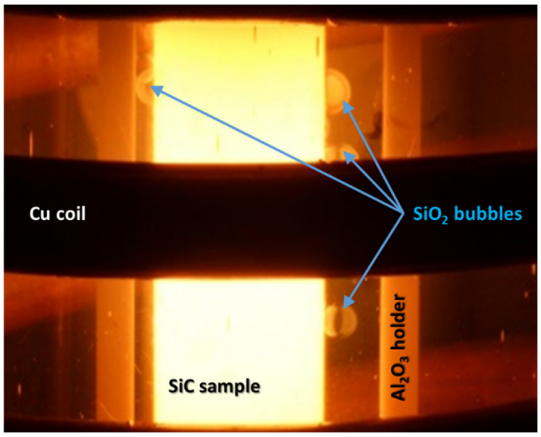

(**c**) SiC-04

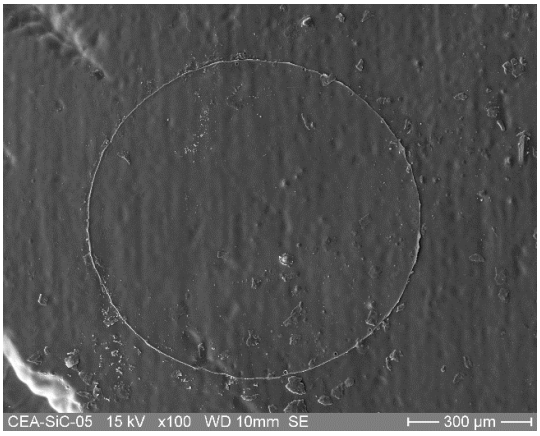

(**d**) SiC-05

Figure 9. Bubble formation at oxidized SiC surfaces: SEM images (**a**,**b**,**d**) and video snapshot taken during test SiC-04 (**c**).

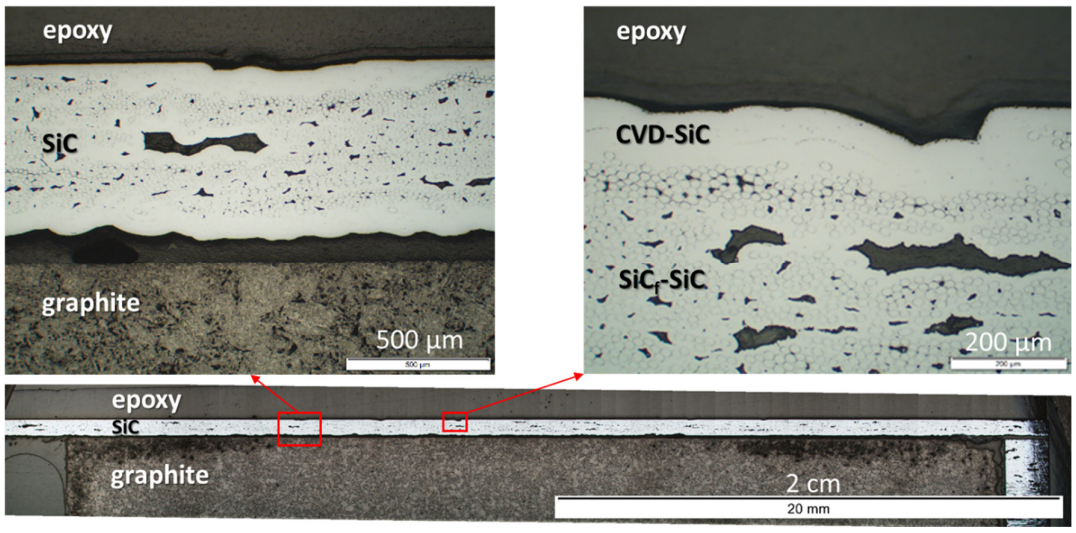

(**a**) SiC-03: Optical micrographs of longitudinal cross section

Figure 10. *Cont.*

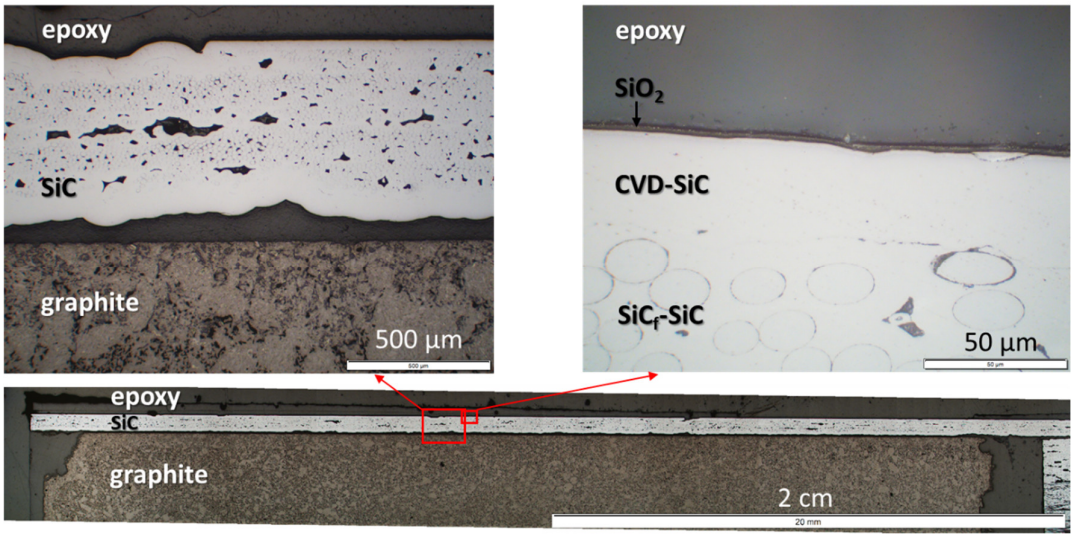

(**b**) SiC-04: Optical micrographs of longitudinal cross section

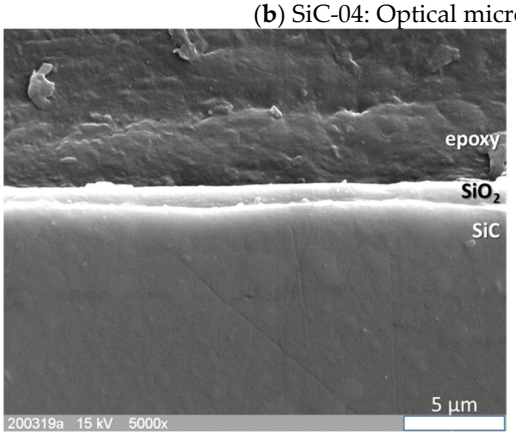

(**c**) SEM image of silica scale on sample SiC-03

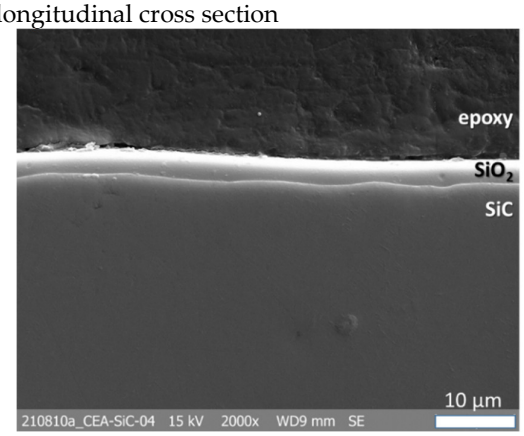

(**d**) SEM image of silica scale on sample SiC-04

Figure 10. OM (**a**,**b**) and SEM (**c**,**d**) images of sample cross sections after 1 h (SiC-03) and 3 h (SiC-04) steam oxidation at 1700 °C.

4.2.2. Mechanical Testing

Figure 11a shows the envelopes of the stress-strain curves measured under tensile loading on the SiC-02 and SiC-05 composite samples after oxidation with the monitoring of the acoustic emission. The reference mechanical behavior measured on unexposed pristine material is also reported. Undoubtedly, the harsh test conditions affected the mechanical behavior with a decrease of the mechanical properties in comparison to the measured reference values (see Table 2). Repeatable mechanical behavior between SiC-02 and SiC-05 samples is observed. The non-linear elastic failure behavior with a pseudo-plateau resulting from matrix micro-cracking is maintained. This is the consequence of low interfacial shear strength due to the presence of the pyrocarbon interphase, which does not seem to be affected by the oxidative atmosphere. Despite the harsh exposure conditions, the fiber–matrix load transfer remains efficient to provide the ability of the composites to accommodate the deformation.

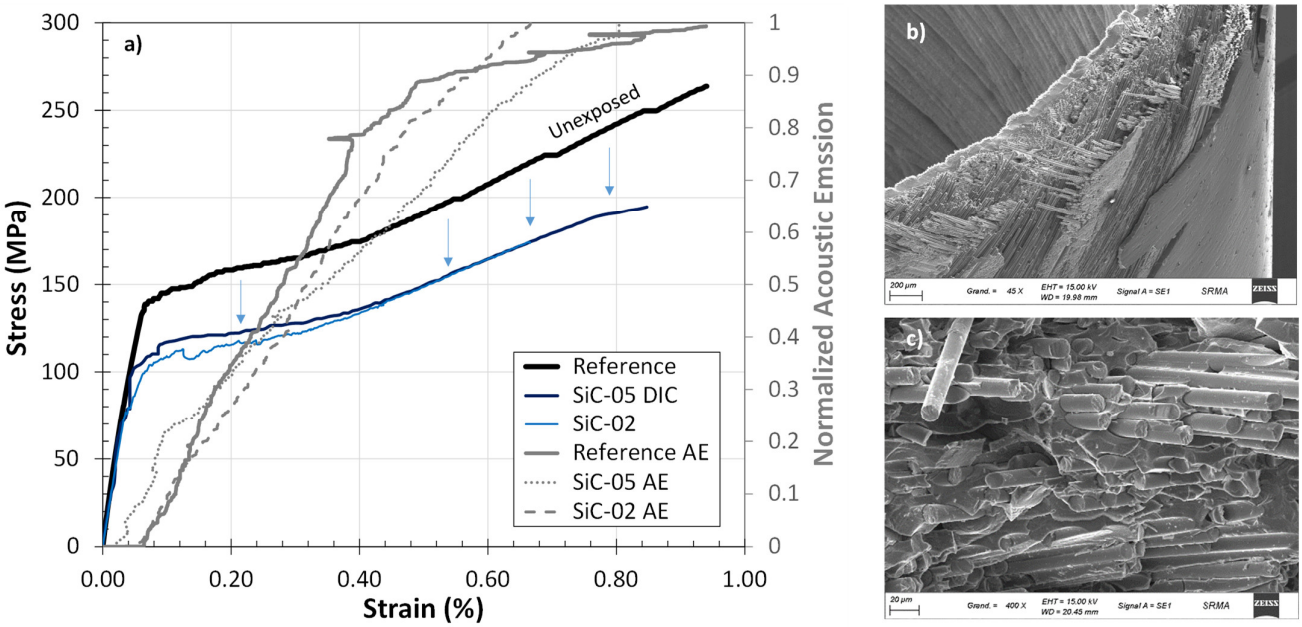

Figure 11. (**a**) Uniaxial tensile stress-strain behavior measured on SiC-02 and SiC-05 samples at ambient temperature after 1 h isothermal oxidation in steam at 1700 °C. The reference stress-strain curve measured on the pristine material is given for comparison. (**b**,**c**) Representative fracture surface SEM images observed at different magnitudes on sample SiC-02.

Table 2. Test characteristics, post-test examinations conducted, and selected results.

Sample	Young Modulus EP (GPa)	Yield Strength σ_y (MPa)	Strain ε_y (%)	Tensile Strength σ_m (MPa)	Strain at Failure ε_m (%)
SiC-02 1 h 1700 °C steam final quenching	227	92	0.056	174	0.66
SiC-05 (DIC) 1 h 1700 °C steam final quenching	235	95	0.047	195	0.85
SiC_f/SiC reference average of 3 samples	260 ± 7	107 ± 15	0.048 ± 0.012	274 ± 6	0.90 ± 0.05

No change in the slope of the normalized acoustic emission signal, AE/AE_{max}, is observed on SiC-02 and SiC-05 samples from the onset of the matrix multi-cracking. This result means that the matrix multi-cracking did not reach saturation up to fracture. On the contrary, the reference behavior exhibits a strong decrease in the AE events occurrence at 0.5% strain that corresponds to 250 MPa, highlighting matrix multi-cracking saturation up to the composite failure. This stress value is higher than the stress at fracture for the SiC-02 and SiC-05 oxidized samples, so the fibers cannot bear such a load for this phenomenon to be observed. SEM post-examination of the fracture surfaces largely exhibit predominant non-brittle areas that are characterized by non-oxidized fiber pull out with high lengths (see Figure 11b,c). A distinction is made between the inner and outer sides, possibly due to the specificity of the oxidizing flux in the furnace. In any case, the overall oxidation kinetics of the external silicon carbide produce a protective silica layer on the surface without evidences of any local penetration. EDS performed on oxidized surfaces show strong oxygen content from the SiC oxidation. However, no oxygen is detected neither on the SiC fibers, nor on the core SiC matrix after a fragment of the matrix has been removed following the mechanical test (see Figure 12). Only carbon and silicon are measured, suggesting that the steam environment did not affect the composite core.

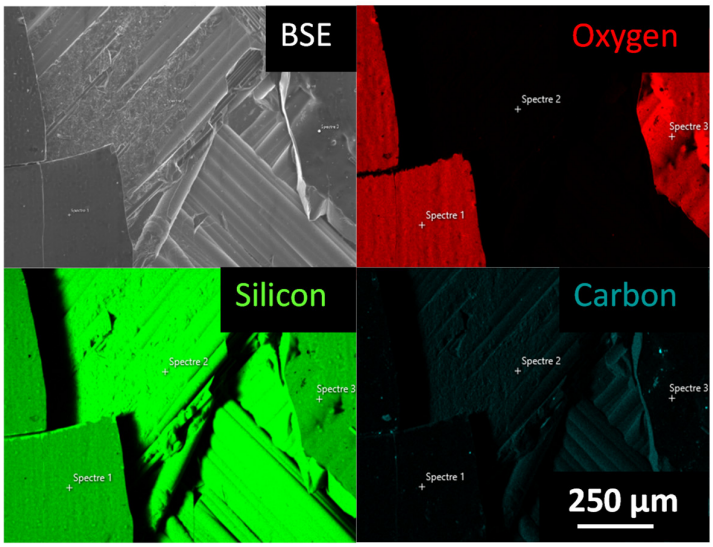

Figure 12. BSE and oxygen, silicon and carbon element mappings (EDS) of the SiC-02 surface after mechanical test up to failure. No oxygen content is measured under the sealcoat, which was removed during the tensile test.

The reduced Young's modulus, the full width at half maximum, the area of the cycles, and the residual strains as a function of the strain level reached before unloading were extracted from the cycled tensile tests, reported in Figure 13. The full width at half-maximum (b) and the area of the cycles (c) are similar, showing no change in the interfacial properties [20] and confirm that the pyrocarbon interface is still effective in acting to deflect micro-cracks. The same goes for the reduced modulus (a), which stays rather unchanged proving the load transfer on the fibers still occurs. Finally, the residual strains after unloading (d), highlighting hindrance of the cracks reclosure or irreversible sliding, are slightly higher after the oxidative tests. This result seems not significant, since it could increase by a factor 3 to 4 in case of oxidative phenomena according to earlier studies [21].

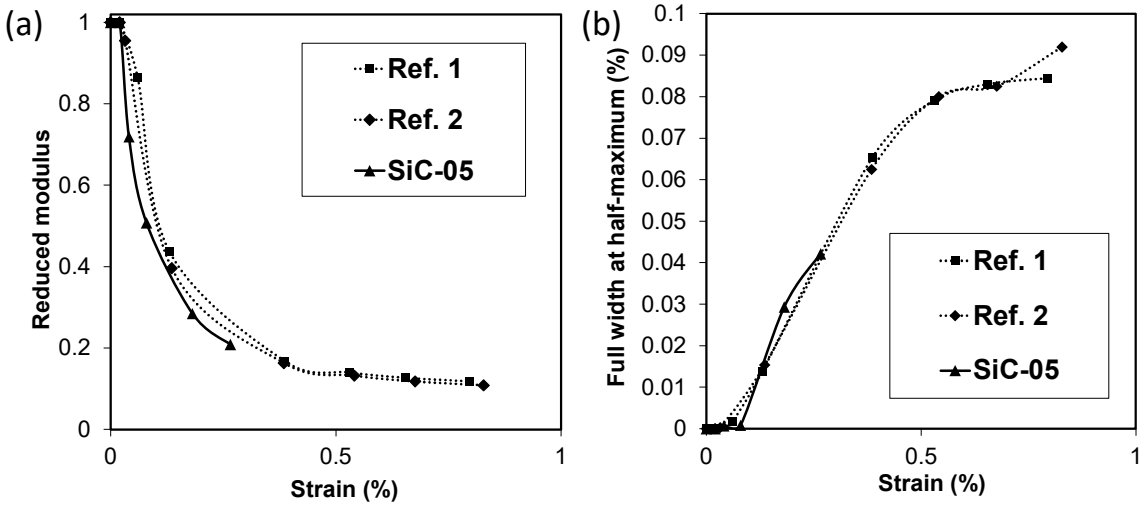

Figure 13. *Cont.*

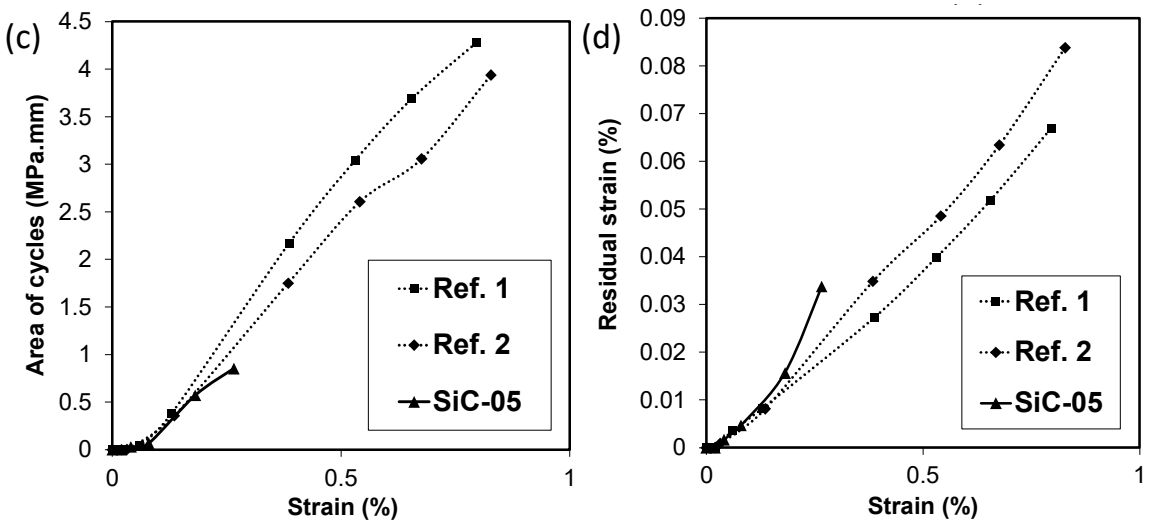

Figure 13. Reduced modulus (**a**), Full width at half-maximum (**b**), Area of the cycles (**c**), and Residual strains after unloading (**d**) as a function of the strain before unloading for reference materials (Ref. 1 and Ref. 2) and SiC-05.

5. Discussion

5.1. Experimental Conditions

The experiments described in this study were conducted with inductive heating; temperature was controlled and measured by a two-color pyrometer, see Section 3 and Figure 2. Due to the very high temperatures investigated, no independent temperature measurement by thermocouples, as usually applied in QUENCH-SR experiments, could be used. Hence, temperature data rely only on pyrometer measurements and on the > 20 years' experience of the operators of the facility. The temperature accuracy of the pyrometer signal is estimated to be ±30 K. This is a clear disadvantage of the test series, resulting in some uncertainties in the quantitative analysis of the results. Furthermore, as seen, e.g., in Figure 4, a certain axial temperature gradient is established during the tests with the maximum in the mid position where the temperature is controlled and measured.

On the other hand, the advantages of test facility and procedure are obvious. The inductive heating of the graphite core is comparable to fuel rod heating and not dependent on changes of the cladding tube properties. It allowed fast and homogenous heating of the samples up to very high temperatures. Hence, for the first time rather prototypical single-rod tests with nuclear grade silicon carbide based composite cladding in steam atmosphere could be conducted up to temperatures of their failure above 1800 °C. Similar experiments with smaller samples had been only conducted by Avincola [16] in the same laboratory. Another big advantage of the QUENCH-SR rig is that no impurities of Al and alkali metals are involved, which may have strong effects on the oxidation kinetics at high temperatures [8]. The samples are directly heated and are surrounded by a cold quartz glass tube, which, by the way, allows the observation of the samples visually and with video camera. Last, but not least, as the name of the facility promises, the samples could be quenched by water of a specified temperature with a predefined flooding rate, which was done during three of the five tests of the series.

5.2. Discussion of Results

No quantitative values of kinetic rate constants are given in this study due to the relatively large sample sizes with significant axial temperature gradients. Anyway, some clear messages can be directly taken from the experimental results. Obviously, the SiC based CMC cladding tubes produced by CEA easily survive a few hours at 1700 °C in oxidizing water steam atmosphere. With the first signs of local alteration at 1820 °C, these new results also highlight in some way the temperature limits of the material to withstand

accident conditions. This is a significant progress compared to classical zirconium alloys, but also to other promising ATF cladding concepts. For instance, one-hour oxidation of Zry-4 would theoretically result in an oxide scale of 2400 µm; and a Zry cladding tube with a typical thickness of 500 µm would be completely oxidized within 2–3 min. In comparison with other ATF cladding concepts, the maximum temperatures that chromium-coated Zr alloys can withstand are around 1200–1300 °C [22] and for FeCrAl alloys 1300–1400 °C [23].

The transient test of this study, and similar ones of earlier experiments with different SiC CMC cladding tubes [24], have shown that the monolithic SiC external layer (here sealcoat) is of decisive importance for the stability of the fiber-matrix composite. Only this layer provides oxidation resistance at very high temperatures, protecting the fibers with their high surface area and easily oxidizing PyC coating. After (local) failure of the external SiC layer, the hydrogen release rate increased sharply by a factor of >30. The fast oxidation of the fiber–matrix composite during the last three minutes of the transient test resulted in the consumption of approximately 50% of tube wall thickness, i.e., of about 300 µm.

On the other hand, no macroscopic degradation of the SiC cladding tubes was observed during and after all isothermal tests at 1700 °C lasting 1 and 3 h, respectively. The originally about 100 µm thick monolithic SiC sealcoat remained continuous and protective. Based on hydrogen release data, 15–25 µm/h thickness loss of SiC can be estimated. This means that this type of cladding should survive those hard conditions for a few hours, which is in accordance with the obtained results. The SiC recession rate calculated based on hydrogen release rates also corresponds with average remaining thicknesses of the monolithic SiC layer of approximately 80 µm after 1 h oxidation and of a bit less than 40 µm after 3 h at 1700 °C in steam. The SiC oxidation, especially the SiO_2 volatilization rates are of course dependent on the experimental boundary conditions like gas flow rate, steam partial pressure, and total pressure as, e.g., described experimentally [16] and by modelling [25]. Other authors explicitly mention SiC recession rates of a few µm per hour at 1700 °C for TRISO (TRi-structural ISOtropic fuel) particles [26] or by thermodynamic and first-principles atomic-scale calculations [19]. These are lower rates than the ones seen in these tests for larger samples of prototypical cladding tube segments.

The rather constant gas release rates, i.e., the oxidations rates, after initiation of the steam flow indicate a fast establishment of equilibrium conditions between parabolic formation and linear volatilization of silica at the given condition: T = 1700 °C, P = 1 bar, P_{H2O} = 0.65 bar, and F_{gas} = 5 cm/s. The measured SiO_2 thicknesses of 1–3 µm correspond to results obtained by other researchers [13,14,16].

The formation of SiO_2 bubbles of different sizes was observed during/after all tests. Such bubbles have been seen also by other researchers and are formed due to the pressure buildup by the formation of gaseous reaction products like H_2 and CO at the SiC/SiO_2 interface [14,16,27,28]. Only during the transient test, significant smoke formation at temperatures above 1800 °C was directly observed through the transparent quartz glass tube. The smoke presumably consisted of volatile and in colder areas condensing and re-oxidizing Si-O-H species like $Si(OH)_4$ and SiO.

Regarding the mechanical behavior, the deterioration observed at 1700 °C is attributed to the tensile strength decrease of the Hi-Nicalon type S fibers coming from the thermal treatment. Sha et al. [29] have already shown that the fibers keep their mechanical properties up to 1600 °C, but lose their mechanical strength between 1600 and 1780 °C. Therefore, the surface parts are excluded, it is assumed that exposing the CVI-SiC/SiC composites to steam alone does not have significant effect on its mechanical performances. Should this result be confirmed, the emergence of the new grade of Tyranno SA4 SiC fiber deemed to have higher crystallite size than the Hi-Nicalon type S would increase the thermal stability of the reinforcements, and, hence, of the composite. The recent capability in producing a damage-tolerant SA4 fiber composite in the laboratory [30] offers a great opportunity to fill this performance gap.

Finally, the thermal shock due to the water quenching does not seem to have significant impact on the mechanical responses, which is consistent with previous results, even though

it may lead to limited matrix multi-cracking (decrease in the composite Young's modulus). Whether the CVI-SiC/SiC specimen were quenched or not, only a single regime of acoustic emission was detected indicating that matrix cracking saturation did not occur up to the ultimate failure [31].

6. Summary and Conclusions

Five oxidation experiments were performed at very high temperatures in steam atmosphere using advanced nuclear grade SiC_f/SiC CMC cladding tube segments. The samples were heated internally by HF induction of a cylindrical graphite susceptor, with no evidence of chemical interaction between the SiC cladding and the graphite susceptor. A transient experiment was carried out until serious local degradation of the sample at maximum temperature of approximately 1845 °C. The degradation was caused by locally complete consumption of the external CVD-SiC sealcoat resulting in steam access to the fiber-matrix composite with enhanced oxidation kinetics. Approaching these very high temperatures was accompanied by accelerated gas release mainly of H_2 and CO_2, as well as the formation of surface bubbles and white smoke.

Three isothermal tests for one hour and one test for three hours at 1700 °C in steam with final quenching by water and cool-down in inert atmosphere, respectively, were run under nominally identical conditions. All samples survived the tests without any macroscopic degradation. The SiC sealcoat remained intact and avoided attack of the SiC fibers by steam. The gas release rates as an indicator for the oxidation rate remained low and roughly constant throughout the tests. Quenching by 95 °C hot water and fast cool-down in flowing argon resulted in no visible macroscopic cracks or spallation. Even though a slight decrease in mechanical performances of around 15% is observed, the SiC_f/SiC composite retains its beneficial damage-tolerant behavior after exposure in such harsh oxidizing conditions. The slight degradation of the mechanical properties is probably due to the fibers' strength loss with ageing during annealing at very high temperatures; but further investigations need to be conducted to verify this assumption.

These positive results make it possible to determine the maximum temperature that advanced SiC-based fuel cladding can withstand accident situations in LWRs. They confirm excellent oxidation resistance up to 1700 °C and provide indications on the degradation mechanisms operating beyond this temperature level. A new project named SCORPION in the framework of the Euratom Research and Training Program 2021–2025 was accepted by the EU in February 2022, which will focus on the behavior of silicon carbide materials during operation in nuclear reactors as well as during hypothetical accident scenarios.

Author Contributions: Conceptualization, M.S. and C.L.; methodology, all authors; validation, M.S. and C.L.; formal analysis, M.S and J.B.; investigation, M.S., U.S. and J.B.; resources, M.S. and C.L.; writing—original draft preparation, M.S. and J.B.; writing—review and editing, all authors; project administration, M.S. and C.L.; funding acquisition, M.G. and C.L. All authors have read and agreed to the published version of the manuscript.

Funding: This research has received funding from the Euratom Research and Training Programme 2014–2018 under grant agreement No. 740415 (H2020 IL TROVATORE). It was supported by the Helmholtz (HGF) program NUSAFE at the Karlsruhe Institute of Technology.

Institutional Review Board Statement: Not applicable.

Informed Consent Statement: Not applicable.

Data Availability Statement: Data sharing is not applicable to this article.

Acknowledgments: The authors thank P. Severloh (KIT) for ceramographical examination of the samples, A. Meier (KIT) for the X-ray tomography investigation, S. Le Bras (CEA) for tensile mechanical testing and E. Rouesne (CEA) for the SEM fracture surfaces observation. We acknowledge support by the KIT-Publication Fund of the Karlsruhe Institute of Technology.

Conflicts of Interest: The authors declare no conflict of interest.

References

1. Terrani, K. Accident tolerant fuel cladding development: Promise, status, and challenges. *J. Nucl. Mater.* **2018**, *501*, 13–30. [CrossRef]
2. Steinbrueck, M.; Avincola, V.A.; Markel, I.J.; Stegmaier, U.; Gerhards, U.; Seiferta, H.J. Oxidation of SiCf-SiC CMC cladding tubes for GFR application in impure helium atmosphere and materials interactions with tantalum liner at high temperatures up to 1600 °C. *J. Nucl. Mater.* **2019**, *517*, 337–348. [CrossRef]
3. Doyle, P.; Zinkle, S.; Raiman, S. Hydrothermal corrosion behavior of CVD SiC in high temperature water. *J. Nucl. Mater.* **2020**, *539*, 152241. [CrossRef]
4. Steinbrück, M.; Große, M.; Stegmaier, U.; Braun, J.; Lorrette, C. High-temperature oxidation of silicon carbide composites for nuclear applications. In Proceedings of the TOPFUEL 2021 Conference, Santander, Spain, 24–28 October 2021.
5. Snead, L.; Nozawa, T.; Katoh, Y.; Byun, T.-S.; Kondo, S.; Petti, D. Handbook of SiC properties for fuel performance modeling. *J. Nucl. Mater.* **2007**, *371*, 329–377. [CrossRef]
6. Presser, V.; Nickel, K. Silica on silicon carbide. *Crit. Rev. Solid State Mater. Sci.* **2008**, *33*, 1–99. [CrossRef]
7. Narushima, T.; Goto, T.; Hirai, T.; Iguchi, Y. High-temperature oxidation of silicon carbide and silicon nitride. *Mater. Trans. JIM* **1997**, *38*, 821–835. [CrossRef]
8. Opila, E.; Jacobson, N. Oxidation and corrosion of ceramics. In *Ceramics Science and Technology*; Wiley: Hoboken, NJ, USA, 2013.
9. Roy, J.; Chandra, S.; Das, S.; Maitra, S. Oxidation behaviour of silicon carbide—A review. *Rev. Adv. Mater. Sci.* **2014**, *38*, 29–39.
10. Pham, H.; Kurata, M.; Steinbrueck, M. Steam oxidation of silicon carbide at high temperatures for the application as accident tolerant fuel cladding, an overview. *Thermo* **2021**, *1*, 151–167. [CrossRef]
11. Cao, F.; Hao, W.; Wang, X.; Guo, F.; Zhao, X.; Rohbeck, N.; Xiao, P. Effects of water vapor on the oxidation and the fracture strength of SiC layer in TRISO fuel particles. *J. Am. Ceram. Soc.* **2017**, *100*, 2154–2165. [CrossRef]
12. Opila, E. Variation of the oxidation rate of silicon carbide with water-vapor pressure. *J. Am. Ceram. Soc.* **1999**, *82*, 625–636. [CrossRef]
13. Terrani, K.; Pint, B.; Parish, C.; Silva, C.; Snead, L.; Katoh, Y. Silicon carbide oxidation in steam up to 2 MPa. *J. Am. Ceram. Soc.* **2014**, *97*, 2331–2352. [CrossRef]
14. Pham, H.; Nagae, Y.; Kurata, M.; Bottomley, D.; Furumoto, K. Oxidation kinetics of silicon carbide in steam at temperature range of 1400 to 1800 °C studied by laser heating. *J. Nucl. Mater.* **2020**, *529*, 151939. [CrossRef]
15. Yueh, K.; Terrani, K. Silicon carbide composite for light water reactor fuel assembly applications. *J. Nucl. Mater.* **2014**, *448*, 380–388. [CrossRef]
16. Avincola, V.A.; Grosse, M.; Stegmaier, U.; Steinbrueck, M.; Seifert, H. Oxidation at high temperatures in steam atmosphere and quench of silicon carbide composites for nuclear application. *Nucl. Eng. Des.* **2015**, *295*, 468–478. [CrossRef]
17. Schneider, B.; Guette, A.; Naslain, R.; Cataldi, M.; Costecalde, A. A theoretical and experimental approach to the active-to-passive transition in the oxidation of silicon carbide: Experiments at high temperatures and low total pressures. *J. Mater. Sci.* **1998**, *33*, 535–547. [CrossRef]
18. Braun, J.; Sauder, C.; Lamon, J.; Balbaud-Célérier, F. Influence of an original manufacturing process on the properties and microstructure of SiC/SiC tubular composites. *Compos. Part A Appl. Sci. Manuf.* **2019**, *123*, 170–179. [CrossRef]
19. Rashkeev, S.; Glazoff, M.; Tokuhiro, A. Ultra-high temperature steam corrosion of complex silicates for nuclear applications: A computational study. *J. Nucl. Mater.* **2014**, *444*, 56–64. [CrossRef]
20. Domergue, J.; Vagaggini, E.; Evans, A. Relationships between hysteresis measurements and the constituent properties of ceramic matrix composites: II, experimental studies on unidirectional materials. *J. Am. Ceram. Soc.* **1995**, *78*, 2721–2731. [CrossRef]
21. Braun, J.; Sauder, C.; Rouillard, F.; Balbaud-Célérier, F. Mechanical behavior of SiC/SiC composites after exposure in high temperature liquid sodium for Sodium Fast Reactors applications. *J. Nucl. Mater.* **2021**, *546*, 152743. [CrossRef]
22. Steinbrück, M.; Stegmaier, U.; Große, M.; Czerniak, L.; Lahoda, E.; Daum, R.; Yueh, K. High-temperature oxidation and quenching of chromium-coated zirconium alloy ATF cladding tubes with and w/o pre-damage. *J. Nucl. Mater.* **2022**, *559*, 153470. [CrossRef]
23. Kim, C.; Tang, C.; Grosse, M.; Maeng, Y.; Jang, C.; Steinbrueck, M. Oxidation mechanism and kinetics of nuclear-grade FeCrAl alloys in the temperature range of 500–1500 °C in steam. *J. Nucl. Mater.* **2022**, *564*, 153696. [CrossRef]
24. Steinbrueck, M. *Unpublished Results. High-Temperature Experiments with SiCf-SiC Samples*; Karlsruhe Institute of Technology: Karlsruhe, Germany, 2020.
25. Avincola, V.A.; Cupid, D.; Seifert, H. Thermodynamic modeling of the silica volatilization in steam related to silicon carbide oxidation. *J. Eur. Ceram. Soc.* **2015**, *35*, 3809–3818. [CrossRef]
26. Terrani, K.; Silva, C. High temperature steam oxidation of SiC coating layer of TRISO fuel particles. *J. Nucl. Mater.* **2015**, *460*, 160–165. [CrossRef]
27. Opila, E. Oxidation and volatilization of silica formers in water vapor. *J. Am. Ceram. Soc.* **2003**, *86*, 1238–1248. [CrossRef]
28. Lee, Y.; McKrell, T.; Montecot, A.; Pantano, M.; Song, Y.; Kazimi, M. Oxidation behavior of sintered tubular silicon carbide in pure steam I: Experiments. *Ceram. Int.* **2016**, *42*, 1916–1925. [CrossRef]
29. Sha, J.; Nozawa, T.; Park, J.; Katoh, Y.; Kohyama, A. Effect of heat treatment on the tensile strength and creep resistance of advanced SiC fibers. *J. Nucl. Mater.* **2004**, *329–333*, 592–596. [CrossRef]

30. Braun, J.; Sauder, C. Mechanical behavior of SiC/SiC composites reinforced with new Tyranno SA4 fibers: Effect of interphase thickness and comparison with Tyranno SA3 and Hi-Nicalon S reinforced composites. *J. Nucl. Mater.* **2022**, *558*, 153367. [CrossRef]
31. Lorrette, C.; Guilbert, T.; Bourlet, F.; Sauder, C.; Briottet, L.; Palancher, H.; Bischoff, J.; Pouillier, E. Quench behavior of SiC/SiC cladding after a high temperature ramp under steam conditions. In Proceedings of the Water Reactor Fuel Performance Meeting, Jeju-do, Korea, 10–14 September 2017.